MRS Communications (2018), *8*, 1191–1196

doi:10.1557/mrc.2018.185

MRS Communications

Research Letter

Raman investigation of the air stability of 2H polytype $HfSe_2$ thin films

Antonio Cruz, Materials Science and Engineering Program, University of California, Riverside, CA 92507, USA
Zafer Mutlu*, Department of Electrical Engineering and Computer Sciences, University of California, Berkeley, CA 94720, USA
Mihrimah Ozkan, Department of Electrical and Computer Engineering, University of California, Riverside, CA 92507, USA
Cengiz S. Ozkan, Materials Science and Engineering Program, University of California, Riverside, CA 92507, USA; Department of Mechanical Engineering, University of California, Riverside, CA 92507, USA

Address all correspondence to Cengiz S. Ozkan at **cozkan@engr.ucr.edu**

(Received 26 May 2018; accepted 15 August 2018)

Abstract

Hafnium diselenide ($HfSe_2$) has a high theoretical carrier mobility but is among the most reactive transition-metal dichalcogenides (TMDs). Herein, we have investigated the air stability of 2H polytype $HfSe_2$ single-crystal thin films by spectroscopic and microscopic techniques. Raman spectroscopy measurements in conjunction with atomic force microscopy reveal the formation of selenium-rich blisters on the surface of the crystals upon air exposure. Transmission electron microscopy analysis indicates that 2H-$HfSe_2$ undergoes a spontaneous phase change to 1T-$HfSe_2$. These results offer Raman spectroscopy as a fast, convenient, non-destructive technique to reliably monitor the surface degradation of TMDs and present an opportunity for further study of phase changes in this material.

Introduction

The study of two-dimensional (2D) and layered materials has expanded beyond graphene and the relatively well-researched MoS_2 to include many more transition metal dichalcogenides (TMDs). In the current crop of layered materials, $HfSe_2$ is enjoying renewed interest.[1,2] Studies on the structure and electronic behavior of $HfSe_2$ go back decades,[3–5] and ongoing studies are buoyed both by improvements in synthesis techniques and by some exciting results from both theoretical[6,7] and experimental[8] work. In particular, the predicted $HfSe_2$ room temperature mobility is about 100 times the prediction for MoS_2.[7] HfS_2, a material analogous to $HfSe_2$, was recently shown[8] to exhibit interesting inter-layer transport properties which may lead to new applications. $HfSe_2$ is one of the most reactive layered TMDs, readily forming Se-rich blisters which has been shown to negatively affect performance. By comparison, other layered TMDs such as HfS_2,[9] MoS_2[10] and SnS_2[11] are much more stable. Despite recent seminal work on the Raman characteristics of polymorphic group six-layered TMDs,[12] to our knowledge a systematic Raman study of the 2H and 1T polytypes of any group 4 TMD has not yet been conducted; thus, the differences between their spectra and any related properties remain unexamined in the bulk, few-layer and monolayer regimes.

2H-MX_2 is hexagonal with trigonal prismatic coordination and two layers per unit cell [Fig. 1(a)]. The 2H polytype can be further subdivided into 2Ha, 2Hb and 2Hc polytypes, depending on the stacking order. 2Hc is the most common; 2Ha has been observed only under high-pressure conditions and 2Hb has not yet been observed.[13] Hereafter, the use of "2H" will refer specifically to the 2Hc polytype. Each layer of 2H-MX_2 is made up of a tri-layer (TL) of atomic monolayers. Metal atoms in adjacent TLs sit directly above or below chalcogen atoms such that the unit cell contains two TLs [Figs. 1(b) and 1(c)]. In the octahedrally coordinated 1T polytype [Fig. 1(a)], corresponding atoms in adjacent layers sit directly above each other, and the unit cell is a single layer [Figs. 1(b) and 1(c)]. Within a TL, atoms are covalently bonded, and TLs are held together by van der Waals forces. The bulk 2H polytype corresponds to the D_{6h}^4 ($P6_3/mmc$) space group. Even and odd numbers of layers in few-layer 2H-MX_2 correspond to D_{3d}^3 and D_{3h}^1, respectively. 1T-MX_2 belongs to the space group D_{3d}^3 ($P\bar{3}\,m1$) in both bulk and few-layer forms and its space group symmetry is independent of the number of layers. These symmetries result in the following irreducible representations at the Brillouin zone center[13]:

$$\Gamma_{2H} = A_{1g} + E_{1g} + 2E_{2g} + A_{2u} + 2B_{2g} + B_{1u} + E_{1u} + E_{2u}, \quad (1a)$$

and

$$\Gamma_{1T} = A_{1g} + E_g + 2A_{2u} + 2E_u. \quad (1b)$$

A_{1g} and E_g modes are Raman active for 1T-MX_2 [Fig. 1(d)] whereas 2H-MX_2 has four Raman active modes: A_{1g}, $2E_{2g}$, and

* Work performed during postdoctoral studies at the University of California, Riverside.

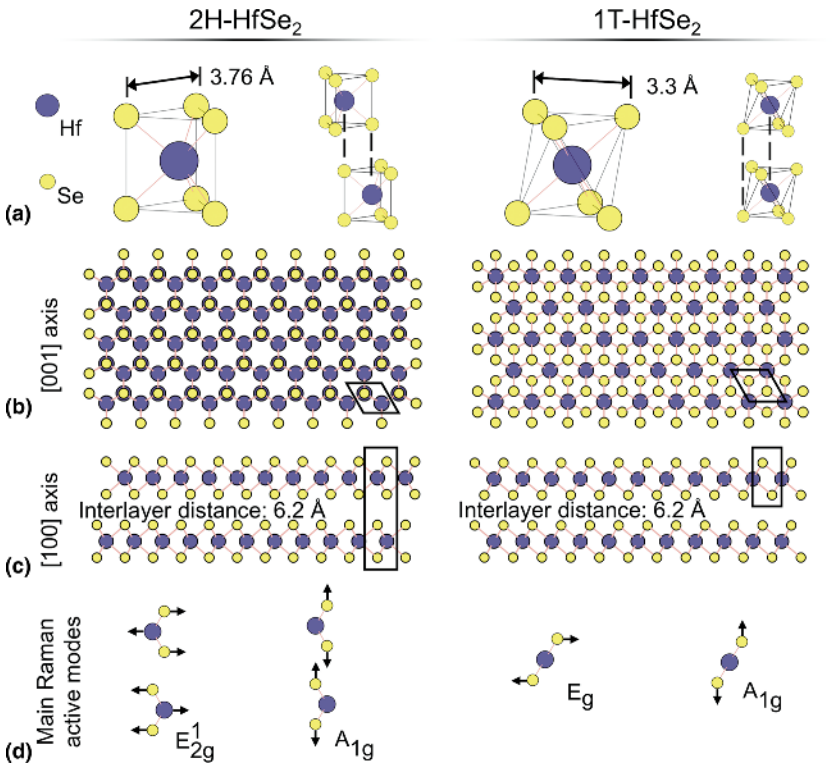

Figure 1. Structure and Raman active vibrational modes of $HfSe_2$. (a) Coordination of metal atoms and lattice parameters in 2H (left) and 1T (right) polytypes. (b) [001] axis and (c) [100] axis views showing the stacking order of the polytypes. (d) Characteristic Raman active modes.

E_{1g}. In 2H-MX_2, A_{1g} and E^1_{2g} are the main Raman modes [Fig. 1 (d)] used for identification because the selection rules operating in the common 180° backscattering Raman setup forbid the E_{1g} mode, and strong Rayleigh scattering at the laser frequency wash out the E^2_{2g} mode without proper filters in place.[13] For a more detailed discussion of the structures and polytypes of TMDs see Refs. 3,5,12,13 and especially the careful group theory work by Ribeiro-Soares et al.[14]

Kim et al. have studied the semiconductor-to-metal transition between the 2H and 1T polytypes of MoS_2.[15] They showed that pristine 2H-MoS_2 Raman spectra exhibit the characteristic A_{1g} and E^1_{2g} peaks. Upon lithium intercalation and deintercalation, regions of 2H-MoS_2 transformed to 1T-MoS_2. Raman spectra of 1T-MoS_2 showed both the absence of the characteristic A_{1g} peak, and the appearance of E_g and J peaks. Ataca et al. performed DFT modeling on select TMDs to search for other stable polymorphic compounds.[16] Their analysis of $TiTe_2$, the only group 4 TMD in the study, indicated that it would be stable in both the 1T and 2H polytypes and would have metallic properties. Most previous studies of $HfSe_2$ were of the 1T polytype. DFT calculations suggest 1T-$HfSe_2$ has a lower energy of formation than 2H-$HfSe_2$,[6] making it the preferred configuration during fabrication. Further DFT modeling[17] explains this preference as group 4 transition metals failing to fill the d_{z^2} subband that splits off at lower energy in the trigonal prismatic configuration. 1T-$HfSe_2$ is an indirect band gap semiconductor with a measured band gap of 1.13 eV.[1,2] Computational work by Zhang et al.[7] has predicted the room temperature mobility of $HfSe_2$ to be above 3500 $cm^2/(V/s)$. This value is an order of magnitude greater than the study's prediction for MoS_2, which is currently one of the most-studied layered materials for devices. They base their prediction on the Takagi model of electron mobility which suggests that in $HfSe_2$, compared to MoS_2, the low electron effective mass in the K–M direction and the relatively weak electron–phonon interaction play significant roles in high mobility. Single crystals of 2H-$HfSe_2$ can be grown using flux zone growth methods.[18] 2H-$HfSe_2$ has an indirect band gap of 1.16 eV.[18] The interlayer distance for 2H-$HfSe_2$ is about 6.2 Å, and the in-plane lattice parameter, corresponding to the d-spacing of {100} planes, is about 3.76 Å.[18] The interlayer distance and in-plane lattice parameter of 1T-$HfSe_2$ are 6.2 and 3.3 Å, respectively.[1,2]

In this study, we report atomic force microscopy (AFM), Raman and transmission electron microscopy (TEM) analyses confirming previous findings that $HfSe_2$ forms Se-rich surface features upon exposure to air. We also performed convergent beam electron diffraction analysis and observed that 2H-$HfSe_2$ undergoes a spontaneous phase change to 1T-$HfSe_2$.

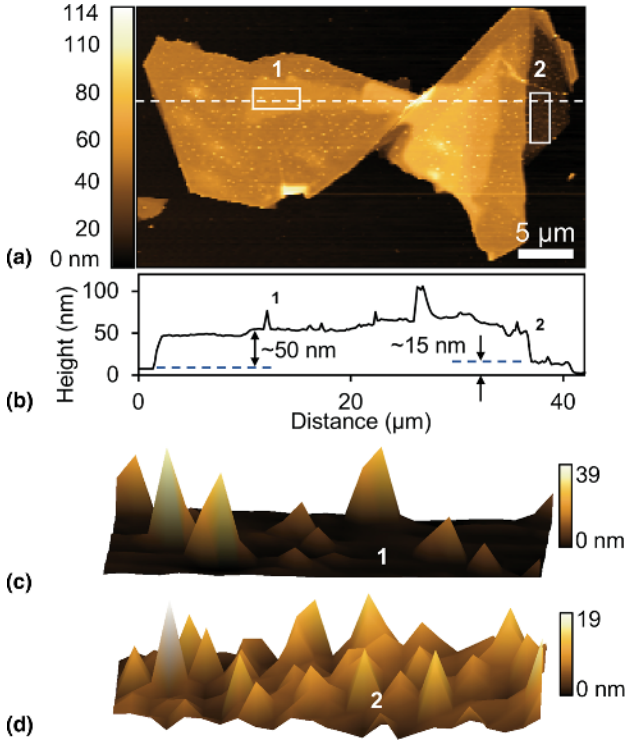

Figure 2. AFM of $HfSe_2$ flake exfoliated in air. (a) AFM height image and (b) corresponding height profile of a $HfSe_2$ flake. (c), (d) 3D AFM height images of the regions 1 and 2, respectively, as demarcated by the rectangle in (a).

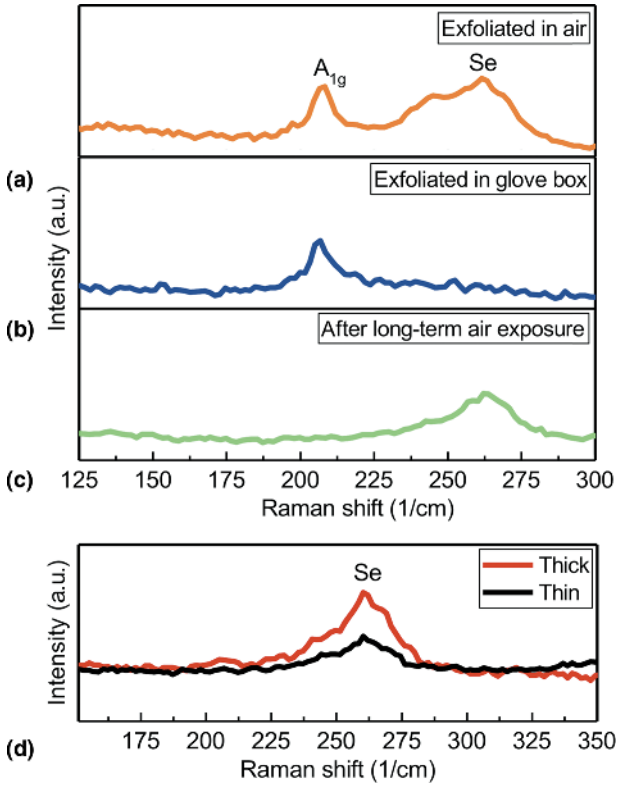

Figure 3. Raman study of air stability of $HfSe_2$. Raman spectra of the $HfSe_2$ flakes taken immediately after exfoliation in (a) air and (b) glove box. (c) Raman spectra of $HfSe_2$ after long-term exposure to air. (d) Raman spectra comparison of the thin and thick regions of a $HfSe_2$ flake after long-term air exposure.

Methods

Materials synthesis

Four-inch silicon wafers with a 300-nm top layer of silicon dioxide were cut into roughly 10×10-mm^2 pieces and cleaned with acetone and isopropyl alcohol to remove any contaminants. $HfSe_2$ and HfS_2 crystals were purchased from 2D Semiconductors. Flakes of each crystal were exfoliated from the bulk and deposited onto the SiO_2/Si substrates using the Scotch Tape method. Exfoliation was typically carried out under ambient atmosphere. In one experiment, samples of $HfSe_2$ were exfoliated inside a glove box, in argon atmosphere. When not in use, samples were kept in desiccators under low vacuum.

For TEM experiments, samples were once again exfoliated with Scotch Tape, then deposited onto 3-mm copper grids with holey carbon mesh. Rather than the tape being peeled away by hand, the tape and grids were washed first with acetone and then with isopropanol. The acetone caused the tape to warp and self-separate from the grid as the adhesive dissolved. The isopropanol helped to further remove contaminants and residues.

Characterization

Thick and thin regions of the samples were identified on optical micrographs by inspection.[19] Raman spectra were gathered with a Horiba LabRAM spectroscope while varying several experimental parameters: sample thickness, laser power and wavelength, exfoliation conditions and time of air exposure. $HfSe_2$ was extremely sensitive to laser exposure (Fig. S1 in Supplementary Information) so spectra were gathered using a low-energy, low-power 785-nm laser at no more than 3 mW to avoid burning the sample. HfS_2 is less sensitive to the laser, and a 532-nm laser at 10–20 mW was used. Previous work by Yumnam et al.[20] suggests this difference in sensitivity may be due to the lower thermal conductivity of $HfSe_2$, resulting in an inability to dissipate the heat generated by the laser quickly enough. Both to quantitatively compare the thicknesses of the analyzed regions and to gather data on the surface morphology, atomic force microscopy (AFM) was performed with an AIST-NT AFM fitted with Bruker NCHV-A silicon AFM tips which had resonant frequencies of around 310 kHz. TEM micrographs and diffraction patterns were gathered on a FEI Titan X-FEG. In particular, selected area electron diffraction (SAED) and convergent-beam electron diffraction (CBED) patterns were gathered to determine the polytype of $HfSe_2$.

Results and discussion

As detailed in the methods section, we mechanically exfoliated samples of $HfSe_2$ onto SiO_2/Si wafers. Using an optical

microscope, we identified flakes by the differences in color and contrast, which has been used reliably with MoS_2 on 300 nm SiO_2/Si.[19] Exfoliated flakes ranged in area from tens to hundreds of μm^2, with lateral sizes of a few μm to tens of μm (Fig. S1 in Supplementary Information).

AFM was performed to characterize the thickness and surface of the flakes. On one large flake, we observed regions of varying thickness, between 10 and 200 nm [Figs. 2(a) and 2(b)]. AFM images of several $HfSe_2$ flakes showed spire-like features over the entire flake surface [Figs. 2(c) and 2(d)]. Other flakes exfoliated under Ar atmosphere in a glove box did not show the spire-like features.

Raman characterization was carried out on several samples, under ambient conditions. In addition to the strong characteristic A_{1g} peak at 199 cm^{-1}, $HfSe_2$ flakes exfoliated in air showed a broad peak around 260 cm^{-1} [Fig. 3(a)]. At room temperature, amorphous selenium has a Raman peak at that frequency.[21] Additionally, Mirabelli et al. previously investigated the air stability of $HfSe_2$[9] and found similar surface features which they characterized as Se-rich blisters. Raman spectra taken immediately after exfoliation in a glove box did not have the broad peak at 260 cm^{-1} [Fig. 3(b)]. After long-term air exposure, however, Raman spectra of all $HfSe_2$ flakes had the amorphous Se peak and no A_{1g} peak [Fig. 3(c)].

AFM of HfS_2 flakes (Fig. S2 in Supplementary Information) did not display such surface features; we observed HfS_2 to be stable in air, which is also consistent with the findings of Mirabelli et al.[9] One explanation for this difference is the lower electronegativity of Se compared to S, making HfS_2 less susceptible to oxidation.[9] A comparison of the surface morphologies of thick [labeled 1 in Fig. 2(c), about 50 nm] and thin [labeled 2 in Fig. 2(d), about 15 nm] regions showed a difference in blister density. AFM data revealed maximum height and root-mean-squared (RMS) roughness differences between the two regions. The thicker region 1 had a maximum blister height of about 39 nm, compared to the maximum 19-nm height of region 2. Their respective RMS roughness values were 4.32 and 2.79 nm, which agrees with previously reported[9] values (Table S1 in Supplementary Information). The Se Raman peaks of thick and thin regions for a single $HfSe_2$ flake were also compared [Fig. 3(d)]. The thicker region had a stronger peak, indicating more Se on the surface. More Se would correlate with having more $HfSe_2$ available during the formation of the blisters.

TEM analysis was carried out to confirm the polytype of exfoliated $HfSe_2$ flakes [Fig. 4(a)]. TEM images of the flake surface revealed amorphousness with many small, misaligned regions, in contrast with the single-crystalline nature of the as-received bulk sample [Fig. 4(b)]. The observed amorphousness is consistent with the presence of amorphous Se on the surface of the flake. SAED [Fig. 4(c)] confirmed that the crystal structure was hexagonal but could not differentiate between

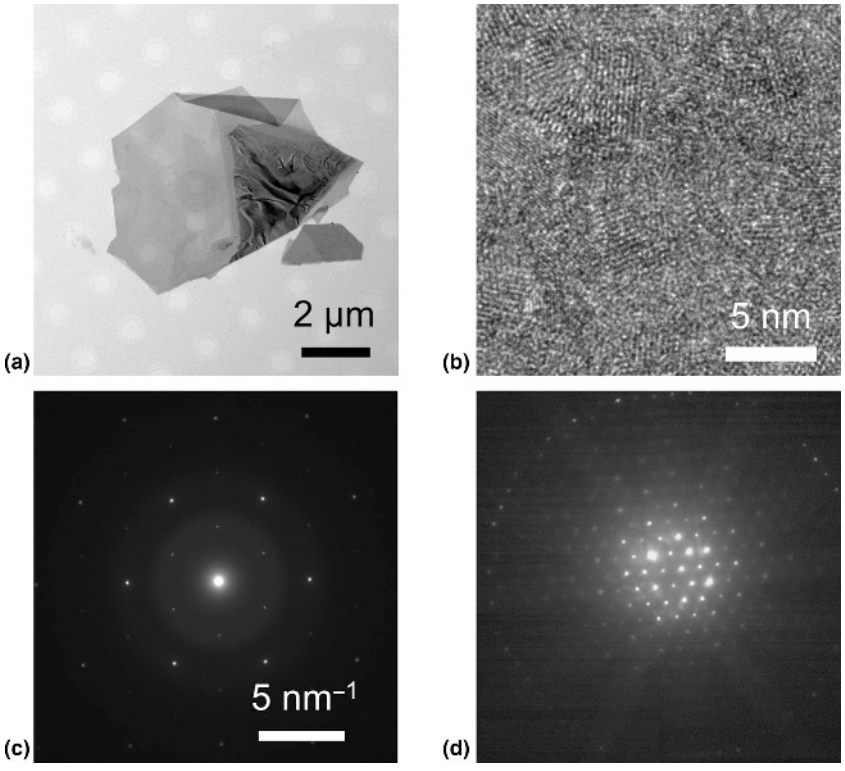

Figure 4. TEM and diffraction analysis. (a) TEM image of $HfSe_2$ flake. (b) TEM image of $HfSe_2$ surface showing amorphousness. (c) SAED pattern showing hexagonal crystal structure. (d) CBED analysis, consistent with 1T polytype of $HfSe_2$.

trigonal prismatic and octahedral coordination of the 2H and 1T polytypes. CBED analysis [Fig. 4(d)] found that the out-of-plane periodicity of the material is 6.2 Å, which is consistent with the 1T polytype since 2H-$HfSe_2$ has two layers per unit cell. XRD performed by the supplier[18] indicate the as-received samples of $HfSe_2$ are of the 2H polytype. The 2H phase as metastable agrees with previous work[6,9] showing that $HfSe_2$ prefers the 1T phase over the 2H phase due to its slightly lower calculated energy of formation. Phase transitions have also been reported to result from strain[22] and lithium intercalation and deintercalation.[15] If the surface reaction and formation of blisters induce strain in the extant $HfSe_2$ crystal, the strain in turn may provide the driving force for the phase change; that is, exposure to air, which causes surface reactions that form the Se-rich blisters, may be the ultimate cause of the transformation. These possibilities suggest methods for phase engineering of polymorphic $HfSe_2$ devices.

Conclusion

We have reported on the air stability of $HfSe_2$. $HfSe_2$ was found to grow spire-like Se-rich surface features upon exposure to air, in agreement with previous work. The morphology of the Se-rich features appeared to depend on the thickness of the flake: approximately 15 nm-thick flakes showed more numerous, 20 nm-tall spikes, whereas approximately 50 nm-thick flakes showed fewer but taller spikes, which were about 40 nm in height. Thicker regions have more $HfSe_2$ present, thus more Se is available for the reaction, allowing growth and coalescence of the spikes. Thinner regions deplete the available $HfSe_2$ sooner, and the reaction stops before the spikes can grow tall. We were able to confirm the presence of Se using Raman spectra. We observed a peak at 199 cm^{-1}, characteristic of $HfSe_2$, and a peak at approximately 260 cm^{-1}, characteristic of amorphous Se. We found one possible method for suppressing the growth of Se-rich spikes on exfoliated $HfSe_2$. By exfoliating $HfSe_2$ in a glove box under Ar, the Se peak disappeared, which we attribute to a suppression of oxidation whereby the formation of blisters is prevented. TEM images showed amorphous structures in the flake, which is consistent with the spontaneous growth of amorphous Se surface features. CBED analysis showed the presence of 1T-$HfSe_2$; the as-received sample was 2H-$HfSe_2$, indicating that a phase transformation took place. We suggest that the 2H phase of $HfSe_2$, due to its higher energy of formation, is metastable, and thus transforms to the 1T phase upon exposure to air. Another possibility is that the formation of Se-rich spikes on the surface of the flakes induces strain in the crystal, and the strain drives the phase change.

Supplementary material

The supplementary material for this article can be found at https://doi.org/10.1557/mrc.2018.185.

Acknowledgments

This work was made possible by support from C-SPIN, a funded center of STARnet, through a SRC program sponsored by MARCO and DARPA. Raman measurements were performed in the ACIF at the UC Riverside. TEM analysis was performed in the CFAMM at the UC Riverside. The authors thank Dr. Krassimir N. Bozhilov for his assistance with TEM analysis.

References

1. L. Yin, K. Xu, Y. Wen, Z. Wang, Y. Huang, F. Wang, T.A. Shifa, R. Cheng, H. Ma, and J. He: Ultrafast and ultrasensitive phototransistors based on few-layered $HfSe_2$. *Appl. Phys. Lett.* **109**, 213105 (2016).
2. R. Yue, A.T. Barton, H. Zhu, A. Azcatl, L.F. Pena, J. Wang, X. Peng, N. Lu, L. Cheng, R. Addou, S. McDonnell, L. Colombo, J.W.P. Hsu, J. Kim, M.J. Kim, R.M. Wallace, and C. Hinkle: $HfSe_2$ thin films: 2D transition metal dichalcogenides grown by molecular beam epitaxy. *ACS Nano* **9**, 474–480 (2015).
3. D.L. Greenaway and R. Nitsche: Preparation and optical properties of group IV–VI2 chalcogenides having the CdI2 structure. *J. Phys. Chem. Sol.* **26**, 1445–1458 (1965).
4. A. Cingolani, M. Lugara, and F. Levy: Resonance Raman scattering in $HfSe_2$ and HfS_2. *Phys. Scr.* **37**, 389–391 (1988).
5. T.J. Wieting and J.L. Verble: Infrared and Raman Investigations of Long-Wavelength Phonons in Layered Materials, in Electrons and Phonons in Layered Crystal Structures (D. Reidel Publishing Company, Dordrecht, 1979), pp. 324–344.
6. F.A. Rasmussen and K.S. Thygesen: Computational 2D materials database: electronic structure of transition-metal dichalcogenides and oxides. *J. Phys. Chem. C* **119**, 13169–13183 (2015).
7. W. Zhang, Z. Huang, W. Zhang, and Y. Li: Two-dimensional semiconductors with possible high room temperature mobility. *Nano Res.* **7**, 1731–1737 (2104).
8. S. Najmaei, M.R. Neupane, B.M. Nichols, R.A. Burke, A.L. Mazzoni, M.L. Chin, D.A. Rhodes, L. Balicas, A.D. Franklin, and M. Dubey: Cross-plane carrier transport in van der Waals layered materials. *Small* **14**, 1703808 (2018).
9. G. Mirabelli, C. McGeough, M. Schmidt, E.K. McCarthy, S. Monaghan, I.M. Povey, M. McCarthy, F. Gity, R. Nagle, G. Hughes, A. Cafolla, P.K. Hurley, and R. Duffy: Air sensitivity of MoS_2, $MoSe_2$, $MoTe_2$, HfS_2, and $HfSe_2$. *J. Appl. Phys.* **120**, 125102 (2016).
10. A.S. George, Z. Mutlu, R. Ionescu, R.J. Wu, J.S. Jeong, H.H. Bay, Y. Chai, K.A. Mkhoyan, M. Ozkan, and C.S. Ozkan: Wafer scale synthesis and high resolution structural characterization of atomically thin MoS2 layers. *Adv. Funct. Matter* **24**, 7461–7466 (2014).
11. Z. Mutlu, R.J. Wu, D. Wickramaratne, S. Shahrezaei, L. Chueh, S. Temiz, A. Patalano, M. Ozkan, R.K. Lake, K.A. Mkhoyan, and C.S. Ozkan: Phase engineering of 2D tin sulfides. *Small* **22**, 12 (2016).
12. X. Zhang, X.-F. Qiao, W. Shi, J.-B. Wu, D.-S. Jiang, and P.-H. Tan: Phonon and Raman scattering of two-dimensional transition metal dichalcogenides from monolayer, multilayer to bulk material. *Chem. Soc. Rev.* **44**, 2757–2785 (2015).
13. M. Samadi, N. Sarikhani, M. Zirak, H. Zhang, H.-L. Zhang, and A.Z. Moshfegh: Group 6 transition metal dichalcogenide nanomaterials: synthesis, applications and future perspectives. *Nanoscale Horiz.* **3**, 90–204 (2017).
14. J. Ribeiro-Soares, R.M. Almeida, E.B. Barros, P.T. Araujo, M.S. Dresselhaus, L.G. Cancado, and A. Jorio: Group theory analysis of phonons in two-dimensional transition metal dichalcogenides. *Phys. Rev. B* **90**, 115438 (2014).
15. J.S. Kim, J. Kim, J. Zhao, S. Kim, J.H. Lee, Y. Jin, H. Choi, B.H. Moon, J.J. Bae, Y.H. Lee, and S.C. Lim: Electrical transport properties of polymorphic MoS_2. *ACS Nano* **10**, 7500–7506 (2016).
16. C. Ataca, H. Sahin, and S. Ciraci: Stable, single-layer MX2 transition-metal oxides and dichalcogenides in a honeycomb-like structure. *J. Phys. Chem. C* **116**, 8983–8999 (2012).

17. C. Gong, H. Zhang, W. Wang, L. Colombo, R.M. Wallace, and K. Cho: Band alignment of two-dimensional transition metal dichalcogenides: application in tunnel field effect transistors. *Appl. Phys. Lett.* **103**, 053513 (2013).
18. Semiconductors: Large size high quality flux zone grown vdW HfSe2 crystals (2018). Available at: http://www.2dsemiconductors.com/hafnium-diselenide-hfse2/ (Accessed April 10, 2018).
19. H. Li, J. Wu, X. Huang, G. Lu, J. Yang, X. Lu, Q. Xiong, and H. Zhang: Rapid and reliable thickness identification of two-dimensional nanosheets using optical microscopy. *ACS Nano* **7**, 10344–10353 (2013).
20. G. Yumnam, T. Pandey, and A.K. Singh: High temperature thermoelectric properties of Zr and Hf based transition metal dichalcogenides: a first principles study. *J. Chem. Phys.* **143**, 234704–8 (2015).
21. K. Nagata, K. Ishibashi, and Y. Miyamoto: Raman and infrared spectra of rhombohedral selenium. *Japanese J. Appl. Phys.* **20**, 463–469 (1981).
22. S. Song, D.H. Keum, S. Cho, D. Perello, Y. Kim, and Y.H. Lee: Room temperature semiconductor – metal transition of $MoTe_2$ thin films engineered by strain. *Nano Lett.* **16**, 188–193 (2016).